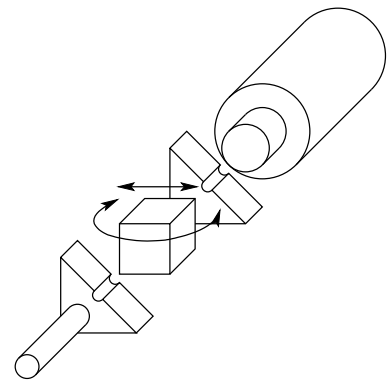


Technical University of Dortmund
Department of Physics
Institute of Experimental Physics III

Computed Tomography
First generation CT for educational purposes

Computertomographie
CT erster Generation für Ausbildungszwecke



Bachelor Thesis

Ole Lemke

Prof. Dr. Dieter Suter, Advisor

Dr. Bärbel Siegmann , Co-Advisor

February the 25th, 2014

Abstract

This work shows a simple setup for a first generation computer tomograph (CT) for educational purposes. ^{137}Cs is used as the gamma radiation source and a scintillation counter as the detector. Rotation and translation of a small sample is realized by two servos, controlled by an Arduino Uno microcontroller board. The count rates are also recorded by the microcontroller board.

Sectional images are generated by a small ruby program with two different filter versions. The output images show the attenuation coefficient μ in relative units.

Zusammenfassung

Diese Arbeit zeigt einen einfachen Aufbau eines Computertomographen (CT) erster Generation für Ausbildungszwecke. Als Strahlenquelle wird ^{137}Cs und als Detektor ein Szintillationsdetektor eingesetzt. Die zu untersuchende Probe kann über zwei Servomotoren, die mit einem Arduino Uno Microcontroller gesteuert werden, rotiert und verschoben werden. Auch die Zählraten werden mit dem Microcontroller aufgenommen.

Aus den Messdaten werden die Schnittbilder mit einem ruby Programm generiert, dem zwei verschiedene Filterversionen zur Verfügung stehen. Die ausgegebenen Bilder geben den Schwächungskoeffizient μ in relativen Einheiten wieder.

Contents

Introduction	1
1 Conceptual basis of CT	3
1.1 Physical foundations	3
1.1.1 Gamma radiation	3
1.1.2 Attenuation of gamma radiation	4
1.1.3 Detection of gamma radiation	5
1.2 Classification of computed tomography	6
1.3 Image generation - filtered back projection	7
2 Implementation	11
2.1 Beam path mechanical control	12
2.1.1 Beam path	12
2.1.2 Mechanics	12
2.1.3 Control electronics	13
2.2 Signal processing	13
2.2.1 Signal parsing and raw data output	14
2.3 Data processing and image generation	15
2.3.1 Loading data	15
2.3.2 Filtered back projection - Version 1	16
2.3.3 Filtered back projection - Version 2	17
2.3.4 Image generation	18
3 Simulation and tests	19
4 Measurements	21
5 Outlook and conclusions	24
Bibliography	i
Appendix	iv

Introduction

For many years past, X-ray techniques have been developed along the same lines, namely the recording on photographic film of the shadow of the object to be viewed. Recently, it has been realized that this is not the most efficient method of utilizing all the information that can be obtained from the X-ray beam.

[...]

In the conventional film technique a large proportion of the available information is lost in attempting to portray all the information from a three-dimensional body on a two-dimensional photographic plate, the image superimposing all objects from front to rear. In order that any one internal structure may be seen, it must clearly stand out against the variations of the materials in front and behind it. [Hou73]

– Sir Godfrey Newbold Hounsfield¹

Computed Tomography (CT) is a non invasive method to produce sectional images. With conventional radiography X-rays or gamma rays are projected through an object on a photographic film. As the absorption of the rays is dependent on the density and structure of the material the structure of the volume is projected onto a plane. It is not possible to reconstruct if an unexposed area is effected by a single object of high density or by many objects of low density in a row.

With CT the rays are projected from different directions through the object and detected by a detector in one plane. The result is a two dimensional absorption profile. A single sectional image can be reconstructed out of this profile using a filtered back projection. This back projection can only be calculated with a computer.

The goal of this work is to develop an experiment for educational purposes at a practical course at TU Dortmund for bachelor and master students. Florian Gubernator and I developed a prototype of a working CT. The experiment is not ready to use for students. But the setup can be the basis to construct a system that can be used in an educational enviroment.

¹Sir Godfrey Newbold Hounsfield shared the 1979 Nobel Prize for Physiology or Medicine with Allan McLeod Cormack for his part in developing the diagnostic technique of X-ray computed tomography. [Raj99]

In this setup we reconstructed a first generation CT, like the one Hounsfield used in 1973. ^{137}Cs is used as the gamma ray source and a scintillation counter as the detector. To take a single sectional image, 1600 measurements have to be made, each measurement takes two minutes. To reduce the effort, we automated the measurement. We programmed an Arduino Microcontroller board to take the data and control two servos for translation and rotation.

To calculate pictures out of the data, we developed a small computer program using the programming language Ruby. In the process of developing this program we developed another program to produce simulated measurements, so we had input data we could trust, because we had no idea if the experiment produces usable measurements.

In the first chapter, this work gives an overview about the physical and mathematical foundations of computed tomography. Discussing all aspects of CT and filtered back projection would exceed the scope of this work, so it will not digress.

The second chapter describes the implementation of the CT in all aspects. With the information given it should be possible to reconstruct the CT.

The third and the fourth chapter present the results of some simulated measurements and some tomographed samples.

The last chapter describes what has to be done to build up a productive system for education.

All source codes and manuals of the developed programs can be downloaded at the project website. <http://projekte.free.de/ct/>

1 Conceptual basis of CT

1.1 Physical foundations

This section gives an overview about the physical foundations needed to understand the experiment.

1.1.1 Gamma radiation

Gamma radiation is electromagnetic radiation with extremely high frequency. Gamma radiation occurs only in conjunction with alpha or beta decay. After alpha or beta decay the atomic nucleus can stay in an excited state. The gamma radiation is produced by the atomic nucleus returning to the ground state or a lower excited state. The spectrum of gamma radiation is discrete.

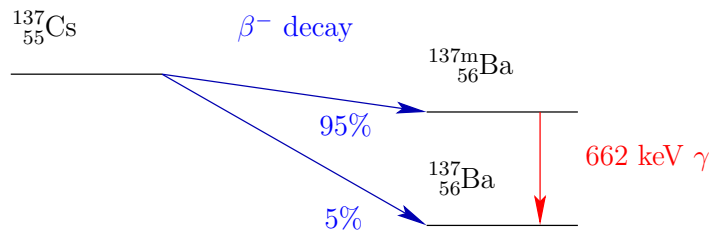
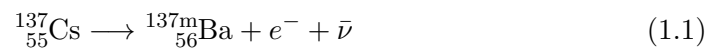


Figure 1.1: Gamma ray emission of ^{137}Cs

$^{137}_{55}\text{Cs}$ has a half life of about 30 years [Unt92]. About 95% decays to $^{137m}_{56}\text{Ba}$ by β^- emission. This meta stable excited state returns to the ground state by about 662 keV gamma ray emission.



1.1.2 Attenuation of gamma radiation

When a γ -photon passes through matter, the intensity decreases exponentially with the thickness of the object and an attenuation coefficient μ .

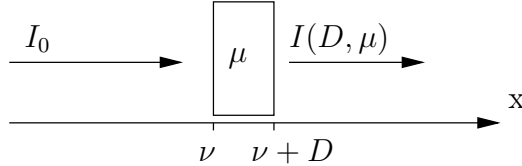


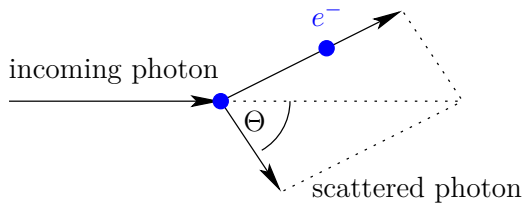
Figure 1.2: Attenuation of gamma radiation

$$I(D, \mu) = I_0 e^{-\mu D} \quad (1.3)$$

The attenuation coefficient μ is depending on the material of the object and on the energy of the radiation. There are three decisive effects of interaction:

Photoelectric effect: The gamma radiation interacts with an atomic electron. The gamma photon is terminated and the kinetic energy of the electron is equal to the gamma energy reduced by the binding energy of the electron.

Compton scattering: The gamma photon interacts with a free charged particle, mostly electrons. After interaction, the gamma energy is reduced equal to the new kinetic energy of the particle and the gamma photon is scattered through an angle Θ .



$$\Delta\lambda = \frac{h}{m_e c} (1 - \cos \Theta) \quad (1.4)$$

Figure 1.3: Compton scattering

Pair production: The γ -photon interacts with a nucleus. If the energy of a γ -photon is equal or higher than $2m_e c^2$, an electron and a positron are created.

The attenuation coefficient in relation to the photon energy of iron and water is shown in figure 1.4. It also gives information which effect contributes to the attenuation.

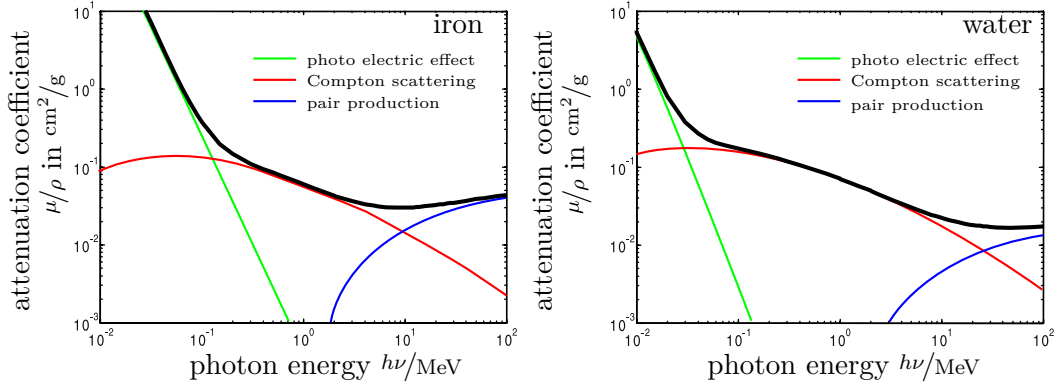


Figure 1.4: Mass attenuation coefficient, $\frac{\mu}{\rho}$, versus incident photon energy for iron and water [Buz08]

1.1.3 Detection of gamma radiation

To detect the gamma radiation a scintillation detector with a NaI crystal as scintillator is used. At scintillation detection an incoming charged particle produces a light flash by exciting atoms or molecules in the scintillator which is detected by a photomultiplier. In the photomultiplier a photon of the light flash reaches the photocathode and electrons are released by the photoelectric effect. The electrons are accelerated in the electric field and reach a dynode (electrode on a higher electric level). At the dynode every electron releases several electrons from the dynode.

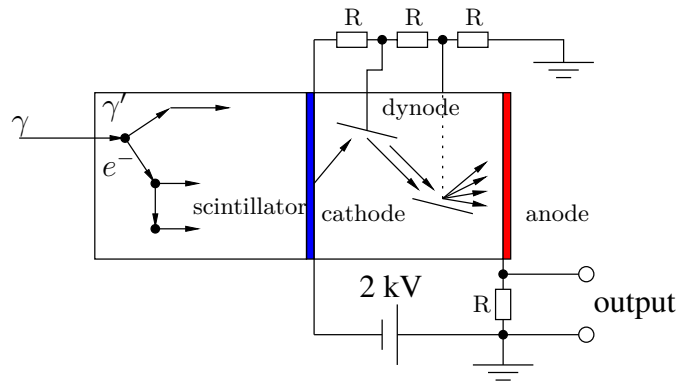


Figure 1.5: Schematic of a scintillation detector

This is repeated several times. The number of electrons grows exponentially with every dynode. At the end, the electrons reach the anode and result in a sharp current pulse. The voltage of the pulse is proportional to the energy of the incoming photon.

The scintillation detector can also detect γ -photons. An incoming γ -photon produces so called secondary electrons in the scintillator material by photoelectric effect or Compton scattering [Dem13] [Kno10]. This is illustrated in figure 1.5.

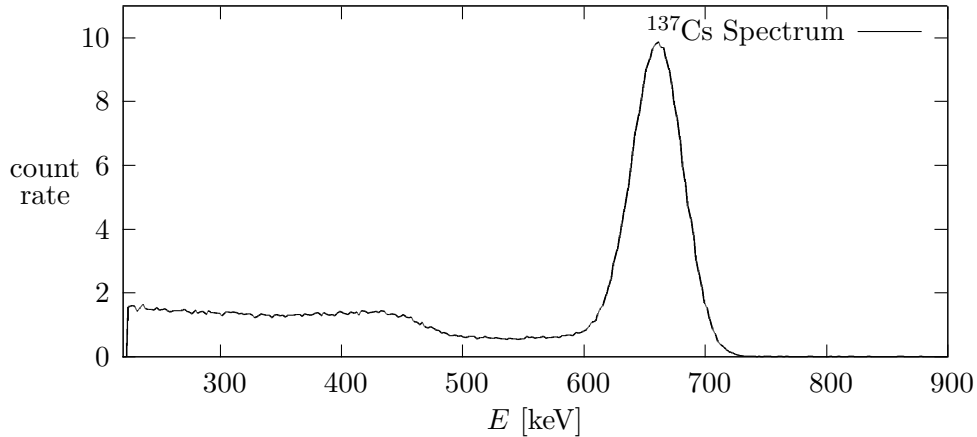


Figure 1.6: Gamma spectrum of ^{137}Cs with count rate in relative units

The discrete spectrum of the ^{137}Cs source is recorded in figure 1.6. The peak at about 662 keV is easily visible. As described the γ -photons can only be detected by the secondary electrons. The main peak is produced by electrons emitted by the photoelectric effect. The continuous spectrum up to about 477 keV is produced by Compton scattering. Equation (1.4) says that the kinetic energy of the emitted electron depends on the scatter angle, up to a maximum of (at $\phi = \pi$):

$$E'_{\text{kin},e,\text{max}} = \frac{2E_{\gamma}^2}{m_e c^2 + 2E_{\gamma}} \quad (1.5)$$

1.2 Classification of computed tomography

Computed tomography is classified in four generations. The first generation of CT used only one detector, in order to reduce the time of measurement an array of up to 30 detectors was used at the second generation. The next step was to expand the angle of opening of the radiation to 40° to 60° and the array contains 500 - 800 detectors. At the third generation of CT translation is not necessary anymore. In 1999 the majority of CTs used in medical environments today are third generation. [Dös99]

Modern commercial CT use X-ray tubes as the radiation source. As detectors solid-state flat-panel detectors are used. [Buz08]

To make CT more compact, a 360° array of about 5000 detectors is used at fourth generation. The detector array stays still and only the X-ray tube rotates. Figure 1.7 gives an overview of the four generations. [Dös99]

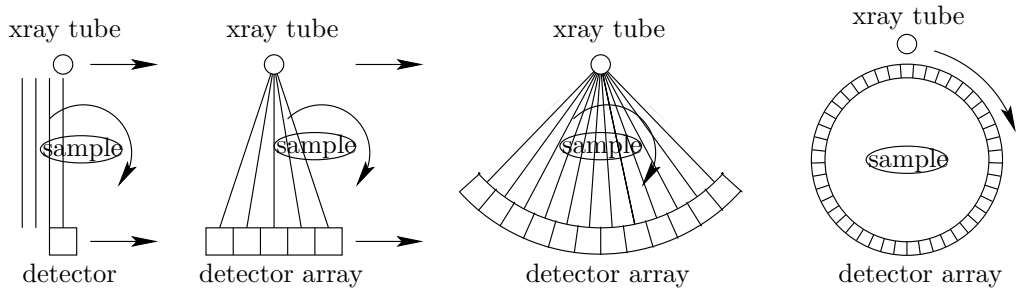


Figure 1.7: The four generations of computed tomography

1.3 Image generation - filtered back projection

An overview of the steps of image generation is shown in figure 1.8. This work will not discuss fundamental principles of mathematics of image generation with CT. These are discussed in the work of Florian Gubernator [Gub14].

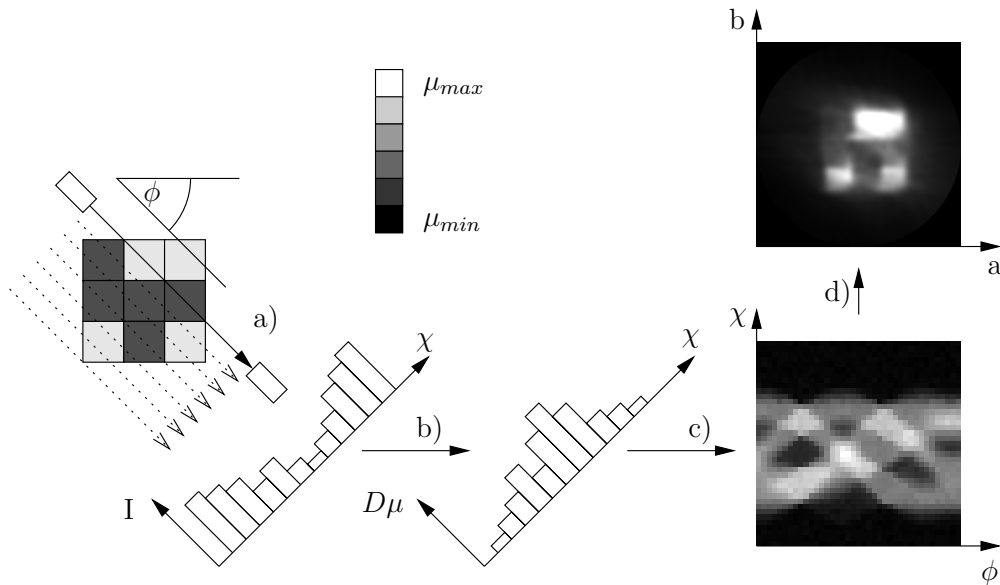


Figure 1.8: Overview of the steps of image generation: a) recording an array of intensity values, b) transforming to an array of $D\mu$, c) forming the Radon space, d) filtered back projection

A measurement produces (rotation steps) \times (translation steps) values of intensity. The values define the Radon space R [Buz08]. According to (1.3) the intensity is transformed to $D\mu$ in relative units.

$$D\mu = \ln \frac{I_{\max}}{I} \quad (1.6)$$

This transformation is omitted hereinafter, to keep it more simple.

To generate sectional images, the Radon space has to be projected to the image. Each point of the Radon space $R(\phi, \chi)$ is projected as a line l to the image $g(a, b)$:

$$R(\phi, \chi) \longrightarrow l : \lambda \begin{pmatrix} \sin \phi \\ \cos \phi \end{pmatrix} + \chi \begin{pmatrix} \cos \phi \\ \sin \phi \end{pmatrix}, \quad \text{with } l \text{ in } g \quad (1.7)$$

According to (1.7), each point in g is the integral over a curve in the Radon space:

$$g(a, b) = \int_0^\pi R(\phi, a \cdot \cos \phi + b \cdot \sin \phi) d\phi \quad (1.8)$$

These curves in the Radon space are illustrated in Figure 1.8 quite well. Figure 1.9 shows the back projection of a Radon space of the projection of a two-dimensional $\delta(x, y)$ function without filtering. Each point in the image $g(a, b)$ receives non negative contributions from all other points of the original image, because every curve in the Radon space defined in (1.7) intersects every other curve at least one time.

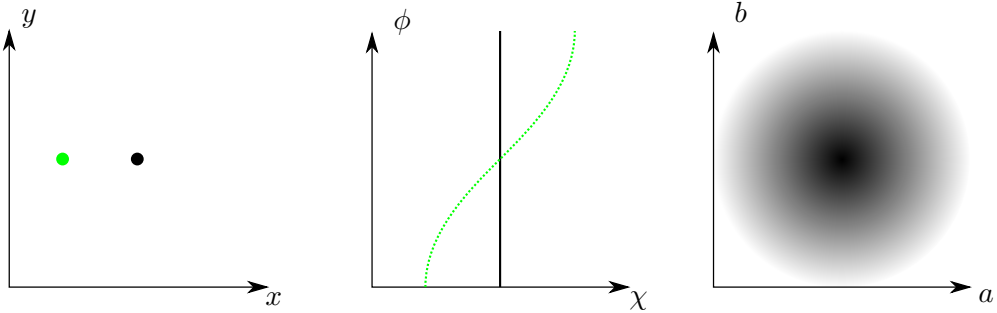


Figure 1.9: Back projection of a δ -Peak without filtering (black) and an example curve (green)

However the intensity of the $\delta(x, y)$ function in the image reduces to

$$g(a, b) = \frac{1}{|(a, b)|}, \quad (1.9)$$

in relative units [Buz08].

To reduce these artifacts it is necessary to add a filter to the back projection. As discussed each point (x, y) in the original image is projected to a curve in the Radon space R . Each point of the curve in R is projected back to the image g as a line through the point (x, y) . If we consider the first line projected through (x, y) , we know that the point will produce positive values to the left and right of the line.

With the filtered back projection, each point of R is not only projected as a (positive) line to g , additional negative values are projected to the left and right of the line. These negative values will eliminate the artifacts produced by the other projections. [Dös99]

A reconstruction of a phantom image with filtered back projection (version 1, see section 2.3.2 for details) and simple back projection in direct correspondence is shown in Figure 1.10.

The filters are described in section 2.3, but not elaborated in further detail. The exact principles of mathematics of filtering would exceed the scope of this work. However, the negative values have to decrease at least proportional to $1/d^2$ or faster.

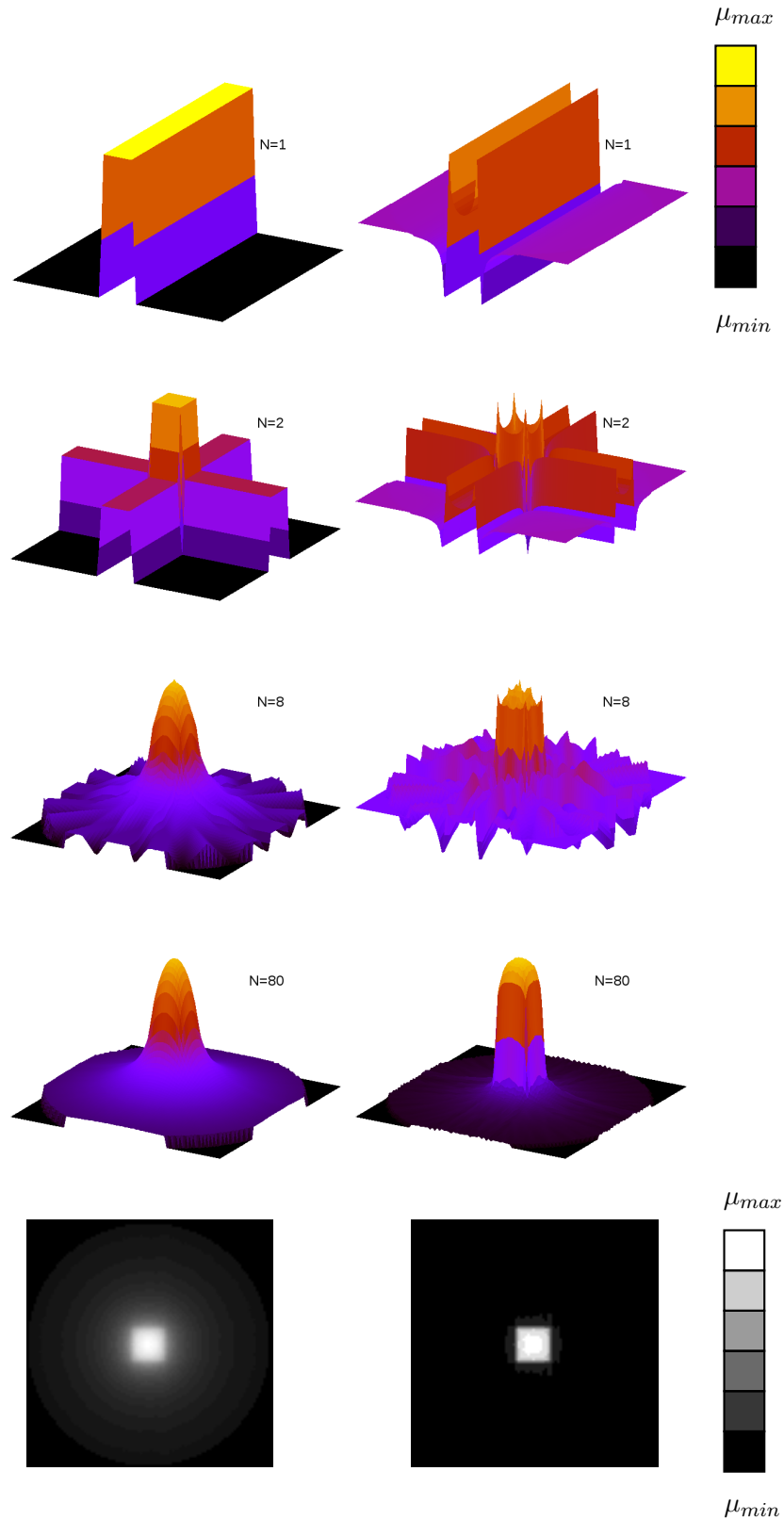


Figure 1.10: Successive reconstruction of simulated projection data. On the left side are the results of simple back projection. On the right side are the results of the filtered back projection version 1 (see section 2.3.2 for details) . All values are in relative units. The number of projections N per row is increased from top to bottom. $N = \{1, 2, 8, 80\}$

2 Implementation

This chapter discusses the implementation of computed tomography. Figure 2.1 gives an overview of the flow of information in the setup. The setup can be divided into three parts: beam path and mechanical control, signal processing and data processing. Each of these parts is discussed in a section.

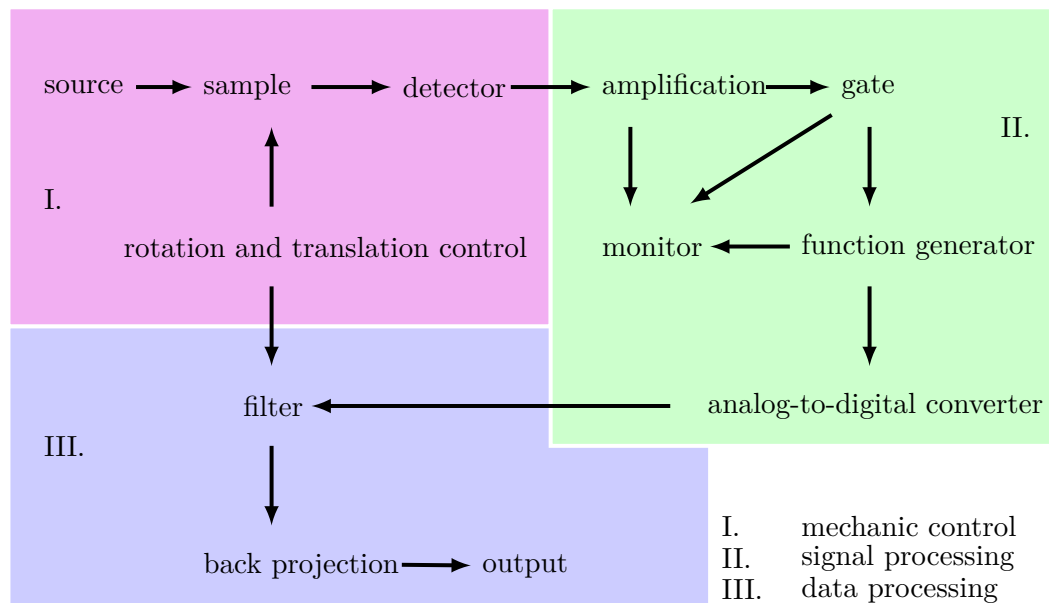


Figure 2.1: Flow of Information in the setup

For all digital controls and analog-to-digital conversion a Arduino Uno board is used. Arduino Uno is a single-board microcontroller, containing an 8 Bit Atmel AVR microcontroller and several analog and digital in- and outputs. The Arduino is programmed via USB with the Arduino IDE using the processing programming language.

All source codes and manuals of the developed programs can be downloaded at the project website. <http://projekte.free.de/ct/>

2.1 Beam path mechanical control

This section describes the setup of the beam path, the mechanics, and control electronics.

According to section 1.2 the setup is a first generation CT. To collect data from many different directions the beam moves in two dimensions, rotation and translation. Because it is a huge effort to move many parts connected to electronics and shielded with lead, we decided to move the object in two dimensions and keep the beam path still.

2.1.1 Beam path

The radiation source is ^{137}Cs . The radiation is emitted at the end of a metal stick containing the Caesium. To get a sharp beam the beam is sent through a 3 mm aperture in a 50 mm thick lead shield. After passing the experimental area the beam is sent through an aperture again.

The apertures collimate the diameter of the beam reaching the detector to 3 mm. The first aperture additionally reduces the scattered radiation. A schematic of the beam path is shown in figure 2.2.

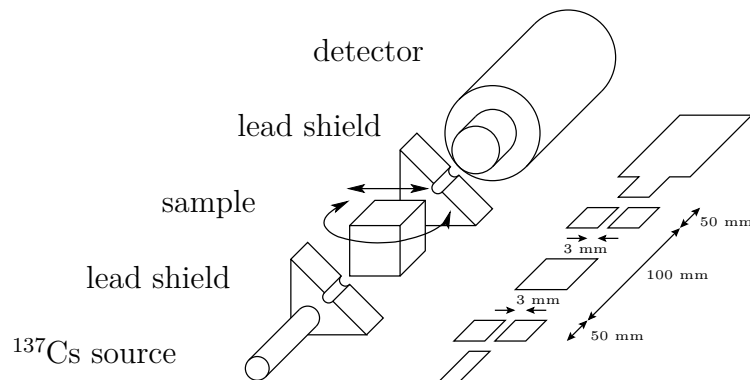


Figure 2.2: Schematic figure of the beam path

2.1.2 Mechanics

The mechanic is implemented in Lego. On the one hand Lego is not the best choice for mechanics, because all mechanic parts have leeway, on the other hand Lego is good for fast prototyping.

The experimental area is limited by the lead shields of the source and the detector. The sample is fixed on a movable table. The table can rotate 200° and move 4.5 cm. The movement is realized by two 180° servos. A top view with opened source and detector shields is shown in figure A.2 in appendix A.

2.1.3 Control electronics

The servos are controlled by the Arduino Uno board. This is shown in figure 2.3. The Servos are connected to the PWM (pulse width modulation) ports P9 and P10. To rotate a servo to a position a PWM command is sent to the servo 50 times in a second. The length of the pulse will determine how far the motor turns. The implementation is realized by using the processing servo library.

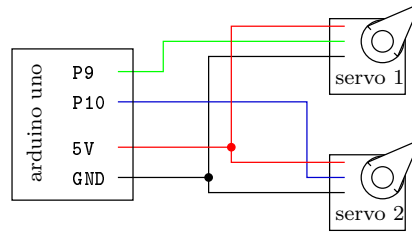


Figure 2.3: Schematic of the servo control electronics

2.2 Signal processing

The schematic of signal processing is shown in figure 2.4 and the timing at several points is shown in figure 2.5. The scintillation detector is powered by 2 kV DC and produces pulses at every event. These pulses can not be parsed by the micro controller directly. The frequency is very high, there is noise and the pulse width is too short.

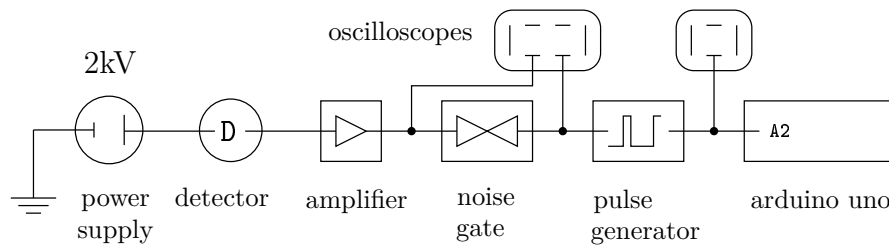


Figure 2.4: Schematic of signal processing

At first the signal is amplified. The amplification is necessary because the noise gate in the next step has a fixed threshold.

After amplifying a noise gate is used to discriminate all pulses and noise lower than 1.2 V from the signal chain. The noise gate is necessary to discriminate the noise on the signal and the detection of secondary electrons emitted by Compton scattering.

To get well defined pulses, a pulse generator produces a rectangular pulse every time a pulse passes the noise gate. The pulse width is $100\ \mu\text{s}$ and the height is $3\ \text{V}$.

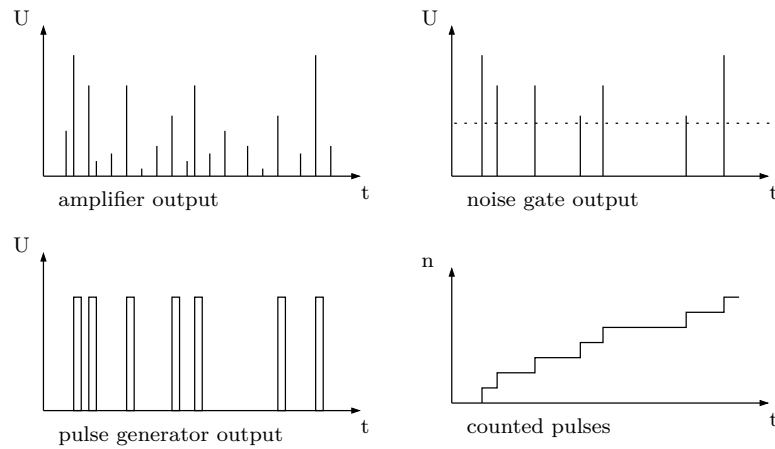


Figure 2.5: Signal timing

2.2.1 Signal parsing and raw data output

The signal is input to Port A2 of the Arduino board. Listing B.1 in appendix B shows the parsing of the signal during measurement, a loop reads the voltage and counts how often the signal switches from $U < 2\ \text{V}$ to $U > 2\ \text{V}$.

The raw data output is sent to the serial port of the Arduino board in CSV format. The layout of the output is `translation,rotation,count_rate` all values are integers, translation and rotation from 0 to 180, `count` ≥ 0 .

2.3 Data processing and image generation

The data processing and image generation is implemented in Ruby. Ruby is a high level and object-oriented programming language.

The program includes several libraries with the following structure.

```
input/                # directory for inputs
lib/                  # directory for libraries
  adjust_measurement.rb # declaration of adjustments
  chunky_png/         # png library
  chunky_png.rb       # png library
  data_object.rb      # class definition data_object
  filter.rb           # filter declaration
  load_data.rb        # data import declaration
  load_data_alt.rb    # alternative data import declaration
  matrixausgabe.rb    # data output declaration
output/              # directory for outputs
tomo.rb              # main program
```

To start the program, the CSV file produced in section 2.2.1 has to be copied to `./input/` and the main program has to be started with:

```
ruby ./tomo.rb <input_file> <output_resolution>
           [<'first' | 'second'>] [<comment>] [<angle correction>]
```

2.3.1 Loading data

The CSV file in the `./input/` directory is parsed and the values are stored in a new data format. Each measurement of intensity is an object on its own containing the translation, the rotation angle and the logarithmic inverse of the count. While storing data, there are made some corrections: the translation is transformed to a scale from -1 to 1 and the angle is transformed from degree to radian. All measurements are stored in an array.

Secondly, the function `adjust_measurement` declared in `./lib/adjust_measurement.rb` converts according to (1.6) the count rate into attenuation in relative units. The implementation is shown in listing B.2 in appendix B.

Notation

In the following some unusual notations are used. The matrix M is notated as

$$M_{ij} = M[i][j],$$

the ceiling and floor function are notated as

$$\text{ceil}(a) = \lceil a \rceil$$

$$\text{floor}(b) = \lfloor b \rfloor.$$

2.3.2 Filtered back projection - Version 1

All values of the projection are stored in a matrix R . This matrix represents the projection data of the objects in the Radon space $\phi \times \chi$. With the filter function f_1 a filtered matrix S is produced.

$$f_1(d) = \begin{cases} 1 & d = 0 \\ -\frac{1}{k_1 \cdot d^2} & d \neq 0 \end{cases} \quad (2.1)$$

$$S[\phi][\chi] = \sum_i R[\phi][i] \cdot f_1(\chi - i) \quad (2.2)$$

In a certain way, S represents the projection data of the objects minus the artifacts. The filter function f_1 and the factor k_1 we determined empirically. Additionally, k_1 depends on the step size of the recorded intensities.

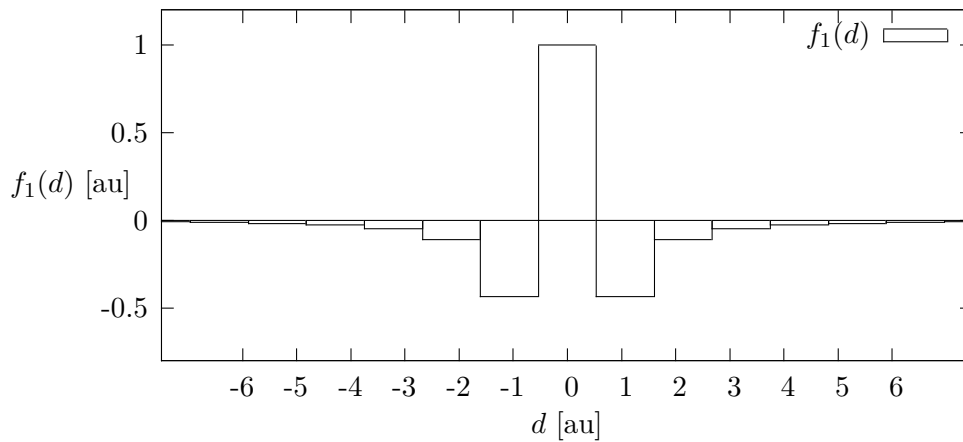


Figure 2.6: Filter function f_1 , with $k_1 = 2$

The back projection is done as described in (1.8). However, S is not a continuous function, we had to add an interpolation to the projection:

$$dx = a \cdot \cos i + b \cdot \sin i$$

$$G[a][b] = \sum_i S[\lfloor dx \rfloor][i] + (S[\lfloor dx \rfloor][i] - S[\lceil dx \rceil][i]) \cdot (dx - \lfloor dx \rfloor) \quad (2.3)$$

It should be noted the projection (2.3) requires that the resolution of the image in the Radon space is equal to the resolution of the output image. For higher output resolutions, the projection has to be supplemented by

$$i' = i \cdot \frac{\text{input_resolution}}{\text{output_resolution}} \quad (2.4)$$

The implementation of (2.3) is listed in listing B.3 in appendix B. Note that the names of variables might differ and the origin of the coordinate system is shifted. `$angle_correction` is a correctional factor which is necessary because the angles in the CSV output are not exact.

2.3.3 Filtered back projection - Version 2

As Florian Gubernator described [Gub14] we employed a second method which has the interpolation included to the filter function f_2 which is also determined empirically.

$$f_2(d) = e^{-d^2} \cdot (1 - (d \cdot k_2)^2) \quad (2.5)$$

The included interpolation is shown in figure 2.7. The sum of the functions

$$\sum_{i=-4}^4 f_2(d+i) \quad (2.6)$$

produces a horizontal line, so the filtered Radon space becomes a family of continuous functions.

$$S[\phi](\chi) = \sum_i R[\phi][i] \cdot f_2(\chi - i) \quad (2.7)$$

Each data point $r[a]$ is projected to each pixel $G[a][b]$. As described in section 2.3.1 r is a data object including the values `r[a].trans`, `r[a].rot` and `r[a].count` which defines the position and the value in the Radon space R . This allows to use non symmetric or non coherent Radon spaces for back projection.

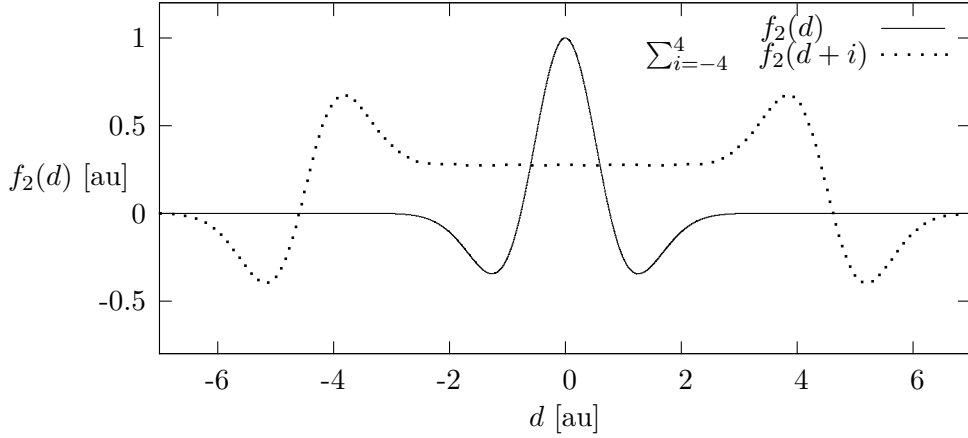


Figure 2.7: Filter function f_2 , with $k_2 = 1.3$

$$d = \left[\begin{pmatrix} \cos(r[i].\text{rot}) \\ \sin(r[i].\text{rot}) \end{pmatrix} \cdot \begin{pmatrix} a \\ b \end{pmatrix} - r[i].\text{trans} \right] \cdot \frac{1}{\text{output_resolution}}$$

$$G[a][b] = \sum_i r[i].\text{count} \cdot f_2(d) \quad (2.8)$$

The implementation of (2.8) is listed in listing B.4 in appendix B. Note that the names of variables might differ and the origin of the coordinate system is shifted.

2.3.4 Image generation

To generate the image from G we used the open source library `chunky_png`. The values of G represent the attenuation coefficient μ in relative units. The relative units depend on adjustments of the radiation source, the chosen filter, the filter constant k and the step size of the recorded intensities. Thus we decided to represent G relative in the image:

$$G_{\max} = 255 \text{ (white)}$$

$$G_{\min} = 0 \text{ (black)}$$

White pixels represent the area of highest absorption, black areas of the lowest absorption.

3 Simulation and tests

Before we implemented the experiment we simulated measurements to develop the software for the back projection. The simulation program generates measurement data from pictures. To estimate if the back projection works with measurements afflicted with errors, we added $\pm 2^\circ$ error on rotation, ± 2 mm error on translation and 5% error on count of every measurement.

The program is implemented with processing language and is described in the work of Florian Gubernator. [Gub14]

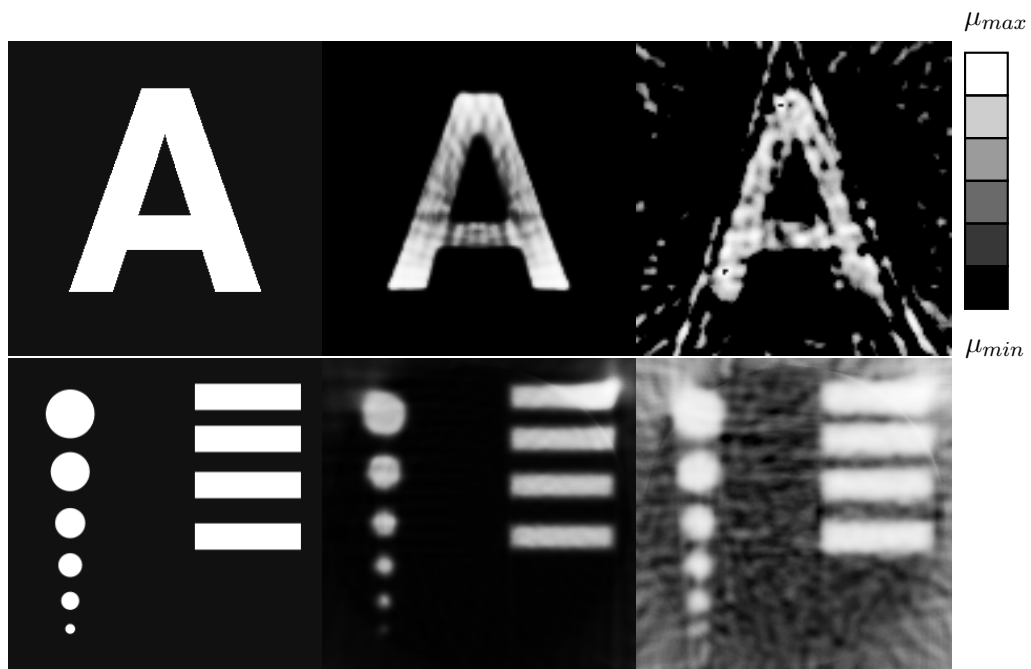


Figure 3.1: Simulation during implementation of the software using back projection version 1 and filter f_1 with $k_1 = 3.2$. From left to right: original image, back projection, back projection with $\sim 5\%$ error on each value and position in Radon space.

Figure 3.1 shows the effect the error takes on the back projection. The effect of different k_1 values with back projection 1 is illustrated in figure 3.2.

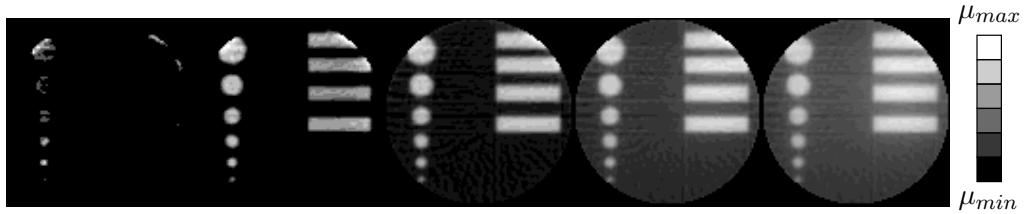


Figure 3.2: Filtered back projection version 1 of simulated projection data with different k_1 values $k_1 = \{2.9, 3.1, 3.3, 3.5, 3.7\}$

The k_1 value defines how strong the filter is. The negative values (projected during filtered back projection) decreases proportional to $1/k_1$ on a given distance.

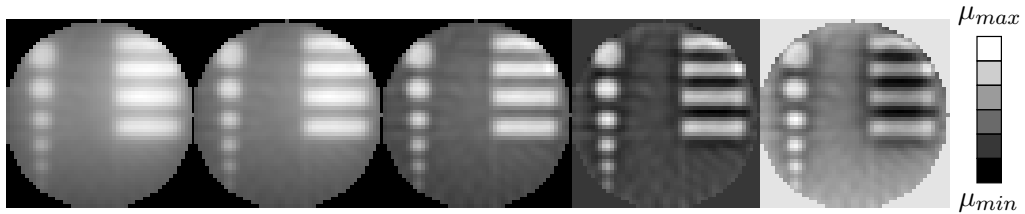


Figure 3.3: Filtered back projection version 2 of simulated projection data with different k_2 values $k_2 = \{1.1, 1.2, 1.3, 1.4, 1.5\}$

With filter version 2 (figure 3.3) the the k_2 value defines the contrast and the edge definition.

4 Measurements

The first sectional picture we took was a cube ($30 \text{ mm} \times 30 \text{ mm} \times 30 \text{ mm}$) with three different layers: iron ($\mu_{Fe, 600 \text{ keV}} = 0.607 \text{ cm}^{-1}$) [NIS95], delrin ($\mu_{Delrin, 600 \text{ keV}} = 0.12 \text{ cm}^{-1}$) [BHS⁺10] and aluminum ($\mu_{Al, 600 \text{ keV}} = 0.211 \text{ cm}^{-1}$) [NIS95].

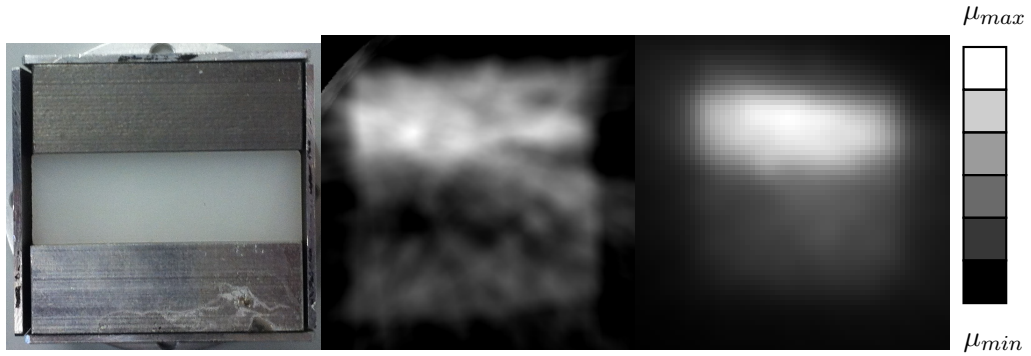


Figure 4.1: Tomography of a cube (one section) with iron (top), delrin and aluminum (bottom). 900 (30×30) intensities were taken with 60 s interval. From left to right: photograph of the sample, back projection version 1 with filter f_1 and $k_1 = 3.3$, back projection version 2 with filter f_2 and $k_2 = 1.2$

With both versions of back projection the iron layer can be distinguished from the other layers. Figure 4.1 shows a photograph of the original cube and the images produced by both versions of back projection.

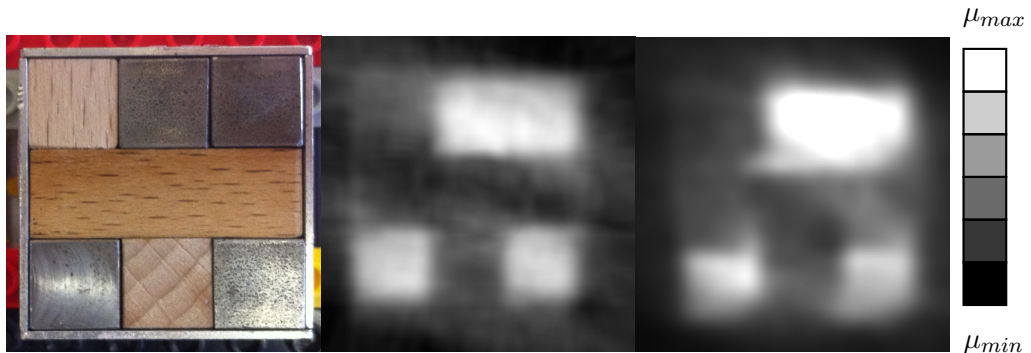


Figure 4.2: Tomography of a cube (one section) with iron (gray) and wood (brown). 1600 (40×40) intensities with 120 s interval were taken. From left to right: photograph of the sample, back projection version 1 with filter f_1 and $k_1 = 3.5$, back projection version 2 with filter f_2 and $k_2 = 1.2$

In the first sectional picture the results of both types of back projection are very noisy with artifacts. So we decided to increase the interval from 60 s to 120 s and the number of measurements from 900 to 1600 for the next picture.

The result is shown in figure 4.2. With both versions of back projection, the artifacts became less and edges became sharper. With both versions the outer aluminum shell is visible in parts. Version 1 shows no visible differences between wood and air which are clearly present in version 2.

Because the increase of the number of measurements to 1600 improved the quality of the image significantly, we decided to increase the number of measurements to 2500. This is the maximum resolution that can be recorded with this setup. As the sample we used four iron sticks with a thickness ranging from 4 mm to 1 mm. The result is shown in figure 4.3. All iron sticks and the aluminum shell are visible with both versions of the filter.

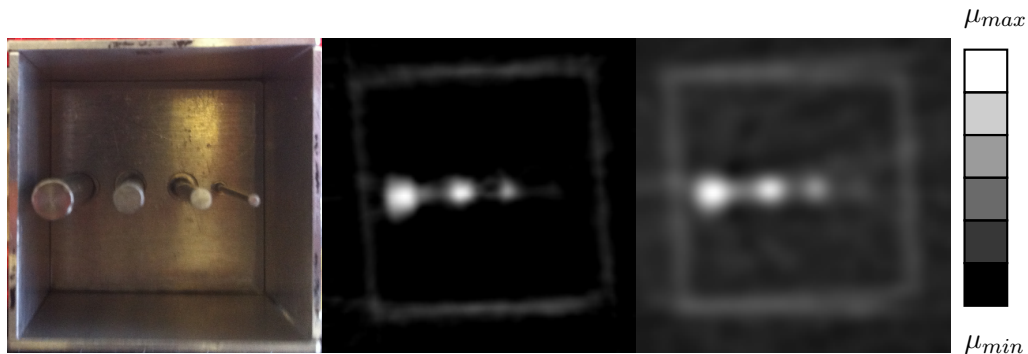


Figure 4.3: Tomography of iron sticks (4 mm, 3 mm, 2 mm and 1 mm). 2500 (50×50) intensities with 120 s interval were taken. From left to right: photograph of the sample, back projection version 1 with filter f_1 and $k_1 = 3.1$, back projection version 2 with filter f_2 and $k_2 = 1.3$

With this measurements we have proven that this setup can map objects down to about 1 mm diameter, if there is a huge contrast between the attenuation coefficients. The next step was to evaluate if this setup can map structures with lower contrast. For this we used the ankle of a lamb (*Ovis aries*) as the sample and took 2500 intensities.

Figure 4.4 shows that there is some internal structure visible, but it can not distinguished between bones and soft tissue.

Error of count rates

To determinate the error of the count rates we collected 2650 count rates in a 120 s interval without an object in the beam path. The mean count rate is given with

$$\bar{n} = (3139 \pm 39) \text{ min}^{-1}.$$

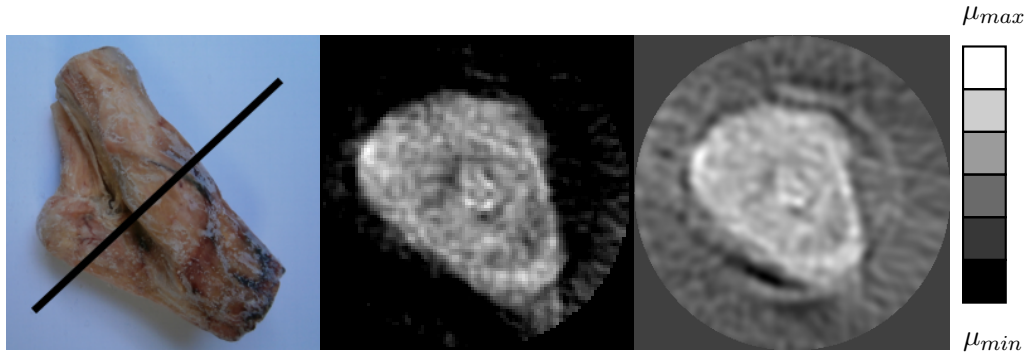


Figure 4.4: Tomography of a ankle of a lamb. 2500 (50×50) intensities with 120 s interval were taken. From left to right: photograph of the sample (the cross section is indicated by the black line), back projection version 1 with filter f_1 and $k_1 = 3.2$, back projection version 2 with filter f_2 and $k_2 = 1.4$

The statistical error of the count rates in the experiment is given with 1.8% (60 s interval) and 1.3% (120 s interval).

The background noise is given with (1501 count rates, 120 s interval)

$$\bar{n}_0 = (43 \pm 4.7) \text{ min}^{-1}.$$

5 Outlook and conclusions

This work has shown that it is feasible to construct a first generation CT based on simple mechanics, control electronics and algorithms for image generation. The result of the experiment is a working CT, built out of parts available in nearly every physics laboratory.

To build a productive system based on this work I propose to optimize a few things:

Radiation source The ^{137}Cs source used in this experiment has an activity of 6.8 MBq. To decrease the time of measurement the radiation source could be replaced by a source with higher activity or a X-ray tube. On the other hand this would increase the radiation exposure of the students and the effort of debugging. At the current setup it is possible to adjust the beam path with a mounted source.

Beam path All parts of the experiment should be fixed on the table. Especially the mount of the radiation source should be constructed in a way that the the source can be easily mounted without adjusting.

Mechanics The Lego mechanics should be replaced by a metal construction with less leeway and more stable parts. The servos and the gear should be replaced by stepper motors and a gear with great translation in order to achieve more exact rotation angles and translations.

Signal processing While building up the CT we didn't order parts for signal processing, we just used parts that were available in the laboratory. All parts of signal processing should be placed in the 19" rack, the noise gate should have a variable threshold and the Arduino Uno should also be mounted in a case with coaxial connectors.

The raw data output should be automatically stored in a CSV file in the `./input/` directory.

Image generation To generate a sectional image with back projection version 1 it takes a few seconds up to a minute to render the image. The calculation time is proportional to

$$\text{input_resolution} \cdot \text{output_resolution}.$$

However the calculation time of back projection version 2 is proportional to

$$(\text{input_resolution} \cdot \text{output_resolution})^2.$$

To render a sectional image it takes about ten hours (with 1600 measurements and 1k×1k pixels output). To reduce the calculation time, the program should be optimized for parallel calculation, so the time could be decreased proportional to n^{-1} on multi core CPUs with n cores.

For using this CT as an experiment for bachelor and master students there should be three main educational aspects:

1. Concept of CT

In preparing the experiment the students learn about the concept of CT especially its first generation.

2. Signal processing

Students should have to wire the whole part of signal processing and should have to adjust all parts.

3. Filtered back projection

The filter functions should be employed by the students.

Bibliography

- [BHS⁺10] BERGER, M. J. ; HUBBELL, J. H. ; SELTZER, S. M. ; CHANG, J. ; COURSEY, J. S. ; SUKUMAR, R. ; ZUCKER, D. S. ; OLSEN, K.: *XCOM: Photon Cross Section Database (version 1.5)*. Gaithersburg, MD, 2010
- [Buz08] BUZUG, Thorsten M.: *Computed Tomography - From Photon Statistics to Modern Cone-Beam CT*. Berlin, Heidelberg : Springer, 2008. – ISBN 978-3-540-39408-2
- [Dem13] DEMTRÖDER, Wolfgang: *Experimentalphysik 4 - Kern-, Teilchen- und Astrophysik*. 4. Aufl. 2014. Heidelberg : Springer-Verlag GmbH, 2013. – ISBN 978-3-642-21475-2
- [Dös99] DÖSSEL, Olaf: *Bildgebende Verfahren in der Medizin - Von der Technik zur medizinischen Anwendung*. Berlin, Heidelberg : Springer, 1999. – ISBN 978-3-540-66014-9
- [Gub14] GUBERNATOR, F.: *Computed tomography with gamma-radiation and Arduino microcontrollers*, Technische Universität Dortmund, Bachelorarbeit, 2014
- [Hou73] HOUNSFIELD, G. N.: Computerized transverse axial scanning (tomography): Part I. Description of system. *British Journal of Radiology* 46 (1973), p. 1016–1022
- [Kno10] KNOLL, Glenn F.: *Radiation Detection and Measurement* -. 4. Edition. New York : John Wiley & Sons, 2010. – ISBN 978-0-470-13148-0
- [NIS95] NIST ; NATIONAL INSTITUTE OF STANDARDS AND TECHNOLOGY (Hrsg.): *Tables of X-Ray Mass Attenuation Coefficients and Mass Energy-Absorption Coefficients from 1 keV to 20 MeV for Elements Z = 1 to 92 and 48 Additional Substances of Dosimetric Interest*. National Institute of Standards and Technology, May 1995. <http://www.nist.gov/pml/data/xraycoef/index.cfm>
- [Raj99] RAJU, T. N.: The Nobel Chronicles. *The Lancet* 354 (9190) (1999), p. 1653–1656
- [Unt92] UNTERWEGER, D. D.; Schima F. J. M. P.; Hoppes H. M. P.; Hoppes: New and revised half-life measurements results. *Nuclear Instruments and Methods in Physics Research A* 312 (1992), p. 349–352

List of Figures

1.1	Gamma ray emission of ^{137}Cs	3
1.2	Attenuation of gamma radiation	4
1.3	Compton scattering	4
1.4	Mass attenuation coefficient, $\frac{\mu}{\rho}$, versus incident photon energy for iron and water [Buz08]	5
1.5	Schematic of a scintillation detector	5
1.6	Gamma spectrum of ^{137}Cs with count rate in relative units	6
1.7	The four generations of computed tomography	7
1.8	Overview of the steps of image generation: a) recording an array of intensity values, b) transforming to an array of $D\mu$, c) forming the Radon space, d) filtered back projection	7
1.9	Back projection of a δ -Peak without filtering (black) and an example curve (green)	8
1.10	Successive reconstruction of simulated projection data. On the left side are the results of simple back projection. On the right side are the results of the filtered back projection version 1 (see section 2.3.2 for details) . All values are in relative units. The number of projections N per row is increased from top to bottom. $N = \{1, 2, 8, 80\}$	10
2.1	Flow of Information in the setup	11
2.2	Schematic figure of the beam path	12
2.3	Schematic of the servo control electronics	13
2.4	Schematic of signal processing	13
2.5	Signal timing	14
2.6	Filter function f_1 , with $k_1 = 2$	16
2.7	Filter function f_2 , with $k_2 = 1.3$	18
3.1	Simulation during implementation of the software using back projection version 1 and filter f_1 with $k_1 = 3.2$. Form left to right: original image, back projection, back projection with $\sim 5\%$ error on each value and position in Radon space.	19
3.2	Filtered back projection version 1 of simulated projection data with different k_1 values $k_1 = \{2.9, 3.1, 3.3, 3.5, 3.7\}$	20

3.3	Filtered back projection version 2 of simulated projection data with different k_2 values $k_2 = \{1.1, 1.2, 1.3, 1.4, 1.5\}$	20
4.1	Tomography of a cube (one section) with iron (top), delrin and aluminum (bottom). 900 (30×30) intensities were taken with 60 s interval. From left to right: photograph of the sample, back projection version 1 with filter f_1 and $k_1 = 3.3$, back projection version 2 with filter f_2 and $k_2 = 1.2$. .	21
4.2	Tomography of a cube (one section) with iron (gray) and wood (brown). 1600 (40×40) intensities with 120 s interval were taken. From left to right: photograph of the sample, back projection version 1 with filter f_1 and $k_1 = 3.5$, back projection version 2 with filter f_2 and $k_2 = 1.2$. .	21
4.3	Tomography of iron sticks (4 mm, 3 mm, 2 mm and 1 mm). 2500 (50×50) intensities with 120 s interval were taken. From left to right: photograph of the sample, back projection version 1 with filter f_1 and $k_1 = 3.1$, back projection version 2 with filter f_2 and $k_2 = 1.3$	22
4.4	Tomography of a ankle of a lamb. 2500 (50×50) intensities with 120 s interval were taken. From left to right: photograph of the sample (the cross section is indicated by the black line), back projection version 1 with filter f_1 and $k_1 = 3.2$, back projection version 2 with filter f_2 and $k_2 = 1.4$	23
A.1	Schematic of the mechanics and the beam path [Gub14]	iv
A.2	Top view photograph of the beam path with opened source and detector shields	v

Appendix A. Figures

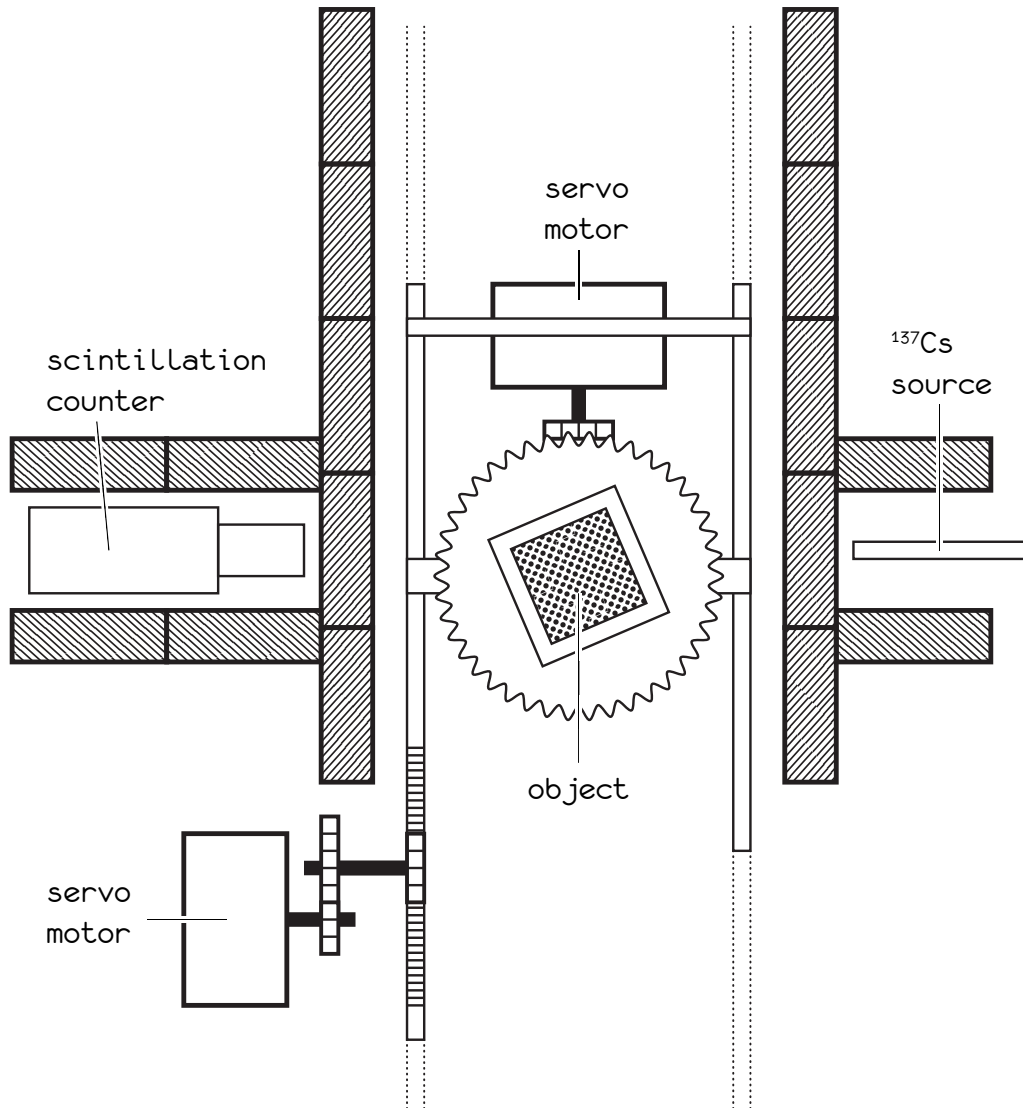


Figure A.1: Schematic of the mechanics and the beam path [Gub14]

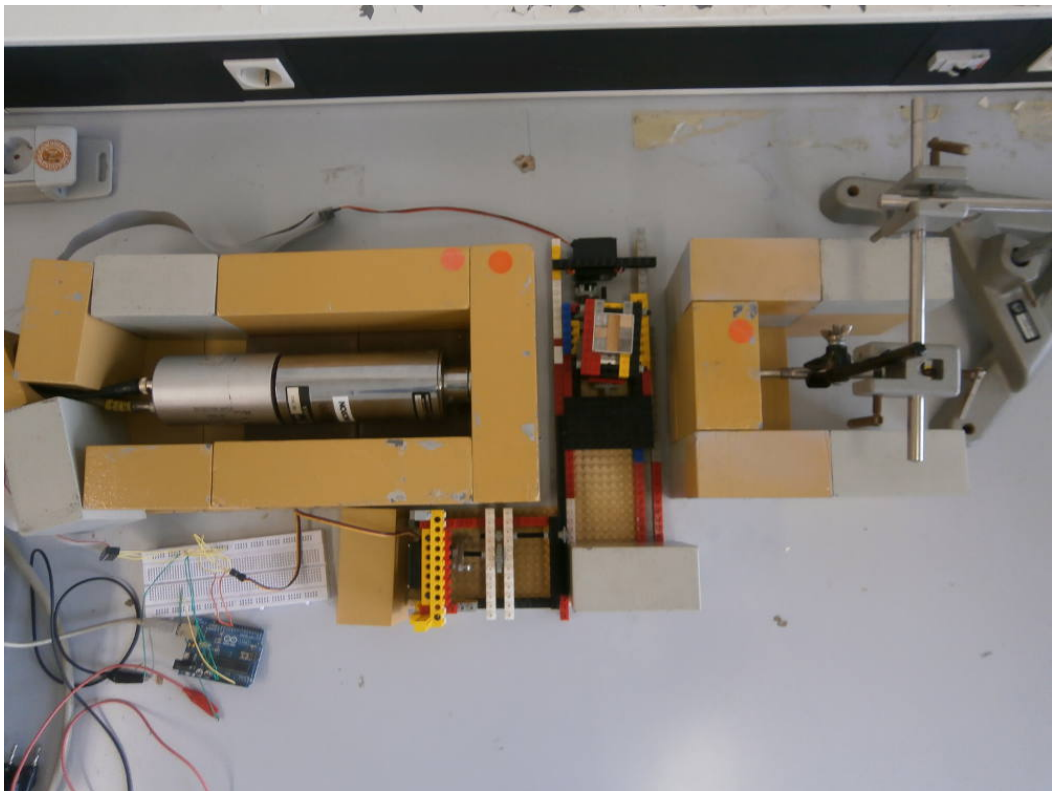


Figure A.2: Top view photograph of the beam path with opened source and detector shields

Appendix B. Listings

Listing B.1: Signal parsing - excerpt from measurement.ino

```
1 while (millis()<time+measureTime*1000){
2   oldSensorValue = sensorValue;
3   sensorValue = analogRead(sensorPin);
4   if (sensorValue>cutOff && oldSensorValue<cutOff){
5     currentCount+=1;
```

Listing B.2: Loading data - excerpt from ./lib/load_data.rb

```
1 File.open('./input/'+ file_name, 'r').each_line do |f|
2   data[k] = Data_object.new
3   data[k].trans = (f.split(",")[0].strip.to_i-90.0)/90
4   data[k].rot = f.split(",")[1].strip.to_i / 180.0 *
      3.14159
5   data[k].count = f.split(",")[2].strip.to_i
6   k += 1
```

Listing B.3: Back projection version 1 - excerpt from ./tomo.rb

```
1 for k in 0..$vector.length-1
2   phi = Math::PI*k*$angle_correction/winkel
3   dx = ((i-(a/2))*Math.cos(phi) + (j-(a/2))*Math.sin(phi)
      )*b/a
4   if dx > -(b/2)+1 && dx < (b/2)-1
5     projection[i][a-j-1] += ($vector[k][[(b/2)+dx.ceil] -
      $vector[k][[(b/2)+dx.floor]]) * (dx - dx.floor) +
      $vector[k][[(b/2)+dx.floor]
```

Listing B.4: Back projection version 2 - excerpt from ./tomo.rb

```
1 r = Vector[x, y]
2 for k in 0..data.length-1
3   u = Vector[Math.cos(data[k].rot), Math.sin(data[k].rot)]
4   d = (u.covector*r)[0]
5   projection[i][j] += filter(d/(output_res*1.0)-data[k].
      trans/2.0, data[k].count )
```

Eidesstattliche Versicherung

Ich versichere hiermit an Eides statt, dass ich die vorliegende Bachelorarbeit mit dem Titel "Computed tomography - First generation CT for educational purposes" selbständig und ohne unzulässige fremde Hilfe erbracht habe. Ich habe keine anderen als die angegebenen Quellen und Hilfsmittel benutzt sowie wörtliche und sinngemäße Zitate kenntlich gemacht. Die Arbeit hat in gleicher oder ähnlicher Form noch keiner Prüfungsbehörde vorgelegen.

Ort, Datum

Unterschrift